


Low leucine levels in the blood enhance the pathogenicity of neonatal meningitis-causing *Escherichia coli*

Received: 30 September 2024

Accepted: 3 March 2025

Published online: 12 March 2025

 Check for updates

Hao Sun^{1,2,6}, Xiaoya Li^{1,2,6}, Xinyuan Yang^{1,2}, Jingliang Qin^{1,2}, Yutao Liu^{1,2}, Yangyang Zheng^{1,2}, Qian Wang^{1,2}, Ruiying Liu^{1,2}, Hongmin Sun^{1,2}, Xintong Chen^{1,2}, Qiyue Zhang^{1,2}, Tianyuan Jia³, Xiaoxue Wu^{1,2}, Lu Feng^{1,2,4}, Lei Wang^{1,2,5}  & Bin Liu^{1,2,4} 

Neonatal bacterial meningitis is associated with substantial mortality and morbidity worldwide. Neonatal meningitis-causing *Escherichia coli* (NMEC) is the most common gram-negative bacteria responsible for this disease. However, the interactions of NMEC with its environment within the host are poorly understood. Here, we showed that a low level of leucine, a niche-specific signal in the blood, promotes NMEC pathogenicity by enhancing bacterial survival and replication in the blood. A low leucine level downregulates the expression of NsrP, a small RNA (sRNA) identified in this study, in NMEC in an Lrp-dependent manner. NsrP destabilizes the mRNA of the purine biosynthesis-related gene *purD* by direct base pairing. Decreased NsrP expression in response to low leucine levels in the blood, which is a purine-limiting environment, activates the bacterial de novo purine biosynthesis pathway, thereby enhancing bacterial pathogenicity in the host. Deletion of NsrP or *purD* significantly increases or decreases the development of *E. coli* bacteremia and meningitis in animal models, respectively. Furthermore, we showed that intravenous administration of leucine effectively reduces the development of bacteremia and meningitis caused by NMEC by blocking the Lrp-NsrP-PurD signal transduction pathway. This study provides a potential strategy for the prevention and treatment of *E. coli*-induced meningitis.

Meningitis is a state of inflammation of the meninges and subarachnoid space that can also involve the cortex and parenchyma of the brain¹. Bacterial meningitis is considered the most severe form of this disease. Despite the availability of antibiotic therapy, the mortality of bacterial meningitis has remained at 20–25% for several decades², and ~50% of survivors sustain permanent/lifelong neurological sequelae, such as hearing loss, developmental delay, and

cognitive impairment^{3–5}. *Escherichia coli* is the most common Gram-negative bacteria that causes meningitis. Among the plethora of serotypes, *E. coli* strains possessing the K1 capsular polysaccharide are more frequently neonatal meningitis-causing *Escherichia coli* (NMEC)⁴. With the increasing emergence of drug resistance, innovative strategies for the treatment of bacterial meningitis are becoming increasingly needed.

¹National Key Laboratory of Intelligent Tracking and Forecasting for Infectious Diseases, TEDA Institute of Biological Sciences and Biotechnology, Nankai University, Tianjin 300457, China. ²The Key Laboratory of Molecular Microbiology and Technology, Ministry of Education, Nankai University, Tianjin 300071, China. ³Shenzhen National Clinical Research Center for Infectious Disease, Shenzhen Third People's Hospital, The Second Affiliated Hospital of Southern University of Science and Technology, Shenzhen, China. ⁴Nankai International Advanced Research Institute, Shenzhen, China. ⁵Southwest United Graduate School, Kunming 650092, China. ⁶These authors contributed equally: Hao Sun, Xiaoya Li. ✉e-mail: wanglei@nankai.edu.cn; liubin1981@nankai.edu.cn

Bacterial meningitis is typically initiated by NMEC through a series of bacterial-host interactions. These interactions encompass vertical transmission of the causative agent from mother to infant and colonization of mucosal surfaces, typically the upper respiratory or gastrointestinal tract^{6,7}. Subsequently, the bacteria invade the intravascular space, surviving and multiplying there, ultimately resulting in bacteremia. NMEC subsequently enters the central nervous system by translocating across the blood-brain barrier (BBB) and induces inflammation in the meninges^{6,8}. Among these steps, a high level of bacteremia is indispensable for NMEC invasion of the BBB, which is a prerequisite for meningitis development⁹. Thus, inhibiting NMEC multiplication in the bloodstream is considered a means of preventing *E. coli* meningitis. However, the bacterial determinants and mechanisms that are essential for inducing a high level of bacteremia remain largely unclear.

The ability to switch between different lifestyles allows bacterial pathogens to thrive in diverse ecological niches¹⁰. Small noncoding RNAs (sRNAs) are robust posttranscriptional regulators of gene expression, typically by base pairing to target mRNAs, and play an important role in the niche adaptation of pathogens^{11,12}. Over the past few years, a growing number of sRNAs that influence bacterial pathogenicity have been identified in *E. coli*^{13–15}. For example, a previous study demonstrated that the sRNA *EsrF* responds to high ammonium concentrations in the colon and enhances the pathogenicity of enterohemorrhagic *E. coli* (EHEC) O157 by promoting bacterial motility and adhesion to host cells¹⁴. Under oxygen-limited conditions, the oxygen-responsive small RNA *DicF* enhances the expression of the EHEC type three secretion system to promote host colonization¹³. *MavR*, a sRNA that is conserved among pathogenic *Enterobacteriaceae*, regulates the expression of genes encoding proteins involved in nutrient acquisition, motility, oxidative stress responses, and attaching and effacing (AE) lesion formation¹⁶. In addition, a previous study identified an mEp460 phage-encoded sRNA, sRNA-17, in NMEC. The expression of sRNA-17 was found to be inhibited in the bloodstream, leading to increased survival of NMEC and enhanced penetration of the BBB¹⁷. Another example in NMEC is the sRNA *Nsr69*, which suppresses flagellin expression and thereby enhances NMEC survival in cerebrospinal fluid (CSF)¹⁸. However, whether sRNAs influence NMEC adaptation to the host remains poorly studied.

During the evolution of NMEC RS218 (serotype O18:K1, a reference strain isolated from the CSF of a neonate with meningitis), 22 genomic islands were acquired, distributed across different regions of the genome, with a total length of ~0.45 Mb¹⁹. These genomic islands are referred to as *E. coli* RS218-derived genomic islands (RDIs)¹⁹. Nearly half of the RDIs have been shown to play a role in meningitis development¹⁹. It is likely that some of these RDIs harbor sRNAs that can regulate NMEC pathogenicity.

Due to their central role in the metabolism of bacteria, nucleotide biosynthesis pathways are strongly linked to the virulence of bacterial pathogens^{20–24}. De novo purine biosynthesis is a major pillar of nucleotide metabolism. The purine biosynthesis pathway leads to the conversion of 5-phosphoribosyl-1-pyrophosphate (PRPP) to inosine 5-monophosphate (IMP) to generate adenine and guanine, which serve as biosynthetic precursors for polymerizing reactions that generate DNA and RNA and as potential energy carriers^{20,25}. The survival and proliferation of bacterial pathogens in the host are influenced by the ability of the pathogens to adjust their metabolism in response to the changing availability of purines within the host environment, especially in the bloodstream, which is characterized by purine-limiting conditions^{23,24}.

Here, we examined how NMEC employs niche-specific strategies to counteract host nutritional immunity. NMEC senses low levels of leucine, a niche-specific signal in the blood, to downregulate the expression of the NMEC-specific sRNA *NsrP* in an Lrp-dependent manner. *NsrP* destabilizes the mRNA of the purine biosynthesis-related

gene *purD*. A decrease in *NsrP* expression in response to low leucine levels activates the de novo purine biosynthesis pathway, resulting in enhanced bacterial pathogenicity in the host. In addition, we showed that the survival and replication of NMEC decreased when the Lrp-*NsrP*-*PurD* regulatory pathway was blocked by increasing the level of leucine in the blood via intravenous administration. This study reveals a potential strategy for using leucine as a potential drug candidate for the prevention and treatment of *E. coli* bacteremia and meningitis.

Results

NsrP is an sRNA that negatively regulates NMEC virulence

By analyzing our previous RNA sequencing (RNA-seq) data of RS218 derived from the blood of mice that were injected with NMEC RS218 via the tail vein¹⁸, we identified a potential NMEC-specific sRNA, which we named *NsrP*. *NsrP* is encoded by RDI 13, which is reportedly involved in the invasion of human brain microvascular endothelial cells (HBMECs), an in vitro BBB model^{19,26}. This finding suggests that *NsrP* may play a role in NMEC virulence. Utilizing an *NsrP*-specific probe, we performed Northern blotting to determine whether *NsrP* is an sRNA transcribed in RS218. The findings showed an RNA band for the RS218 wild-type strain (WT) and the Δ *NsrP* complemented strain (c*NsrP*, which was generated by introducing a plasmid containing *NsrP* with its native promoter into Δ *NsrP*), but not for the Δ *NsrP* strain, indicating that *NsrP* is an sRNA transcribed from the reverse strand of the NMEC RS218 genome (Fig. 1a).

The genomic location of the *NsrP* is shown in Fig. 1b. The 5' and 3' rapid amplification of cDNA ends (RACE) technique was used to determine the transcription start and termination sites of *NsrP*. The results showed that *NsrP* was exactly 244 nucleotides in length, spanning coordinates 2,920,694 to 2,920,937 in the genome (Supplementary Fig. 1a). Since *Hfq* is an indispensable chaperone for both sRNAs and their target mRNAs to facilitate base pairing and to protect sRNAs from degradation by cellular nucleosidases¹⁴, we therefore examined whether *NsrP* is *hfq* dependent. Northern blotting showed that the expression of *NsrP* exhibited no significant difference in the Δ *hfq* strain compared with that in the WT strain (Fig. 1c). Moreover, when bacterial transcription was blocked by rifampicin treatment, the half-life of *NsrP* showed no significant difference in the Δ *hfq* strain compared with that in the WT strain, indicating that *NsrP* is an *Hfq*-independent sRNA (Supplementary Fig. 1b).

To investigate the potential influence of *NsrP* on the pathogenicity of NMEC, we initially performed HBMEC invasion assays. Our findings indicated that the deletion of *NsrP* did not have any discernible impact on the capacity of the bacteria to invade the HBMECs (Supplementary Fig. 1c). To determine the potential role of *NsrP* in the development of bacteremia and meningitis in vivo, we used a mouse model of experimental hematogenous meningitis¹⁸. The results showed that the quantity of Δ *NsrP* in the blood was 7.26 ± 0.30 log CFU/ml, which was 10.42-fold higher than that of the WT strain (6.29 ± 0.22 log CFU/ml) and 11.10-fold higher than that of the c*NsrP* strain (6.25 ± 0.24 log CFU/ml), suggesting that *NsrP* hinders the survival and replication of NMEC within the murine bloodstream (Fig. 1d). In addition, CSF was collected from the mice to assess bacterial penetration across the BBB. The results showed a significant increase in the incidence of *E. coli* meningitis (defined on the basis of positive CSF cultures) in Δ *NsrP*-infected mice compared with that in mice infected with the WT or c*NsrP* strain (Fig. 1e). This finding is consistent with the fact that achieving a high level of bacteremia is a prerequisite for meningitis development for NMEC⁶. Since *NsrP* overlaps with a hypothetical open reading frame (*orf14550*), we mutated the putative start codon of *orf14550* in the chromosome of WT (from ATG to CTG), generating strain *orf14550*^{mut}, and found that this site mutation did not influence the virulence of NMEC (Fig. 1b and Supplementary Fig. 1d, e), suggesting the influence of *NsrP* on the virulence of NMEC is not related with *orf14550*.

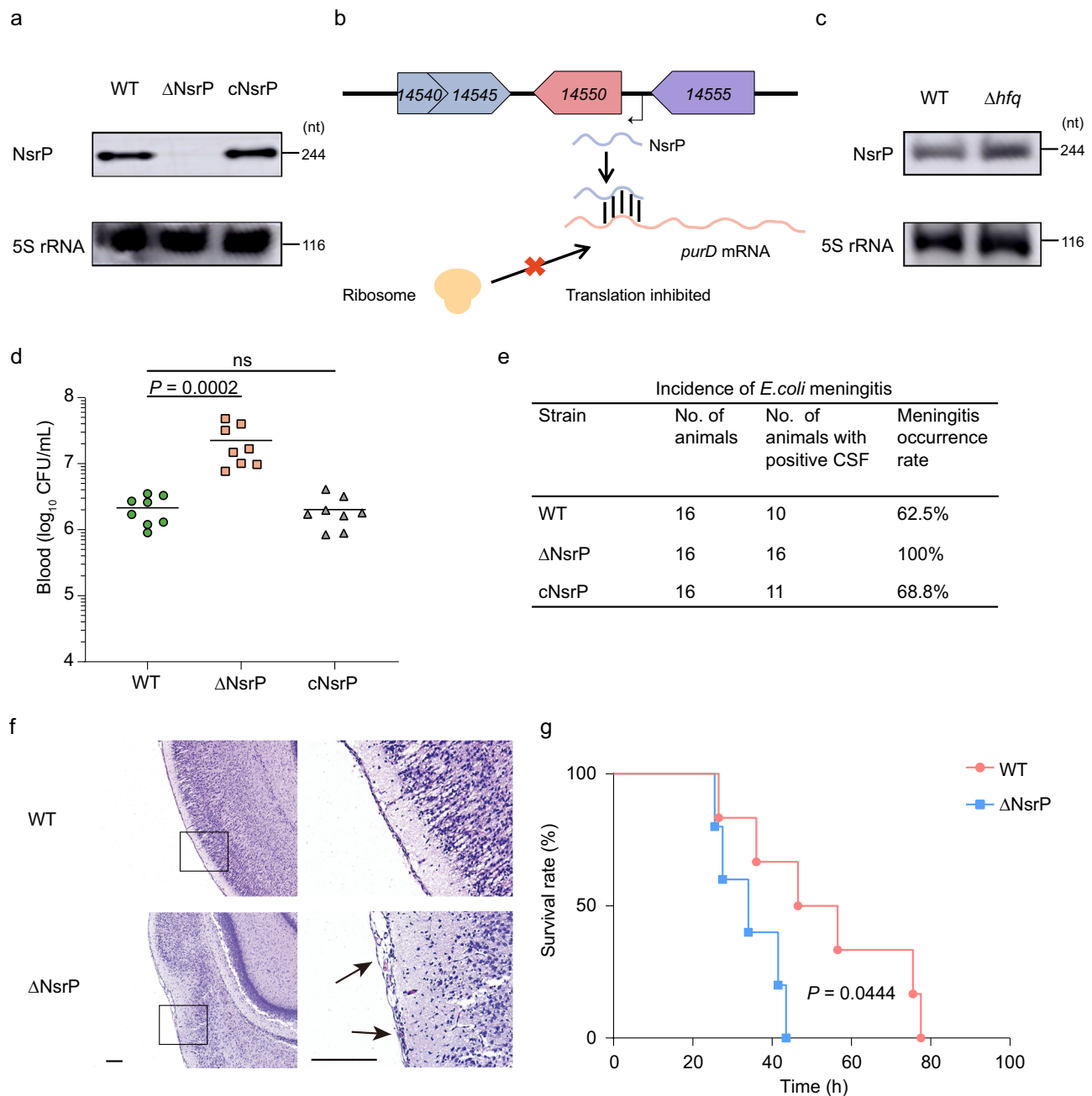


Fig. 1 | NsrP negatively regulates virulence in NMEC RS218. a Northern blotting was performed with a specific probe directed against NsrP sRNA in the NMEC WT, Δ NsrP, and Δ NsrP complemented (cNsrP) strains. 5S rRNA was used as a loading control. **b** The genomic position of the NsrP sequence in the NMEC RS218 genome. **c** Northern blotting for NsrP in RNA preparations from NMEC WT, and Δ hfq. **d, e** Bacterial counts in the blood (CFU/mL, **d**) and meningitis development (**e**) were determined 4 h after intravenous injection of 1×10^6 CFU of the WT, Δ NsrP, or cNsrP strain ($n = 8$ for each group in **d**). CSF culture positivity was defined as meningitis

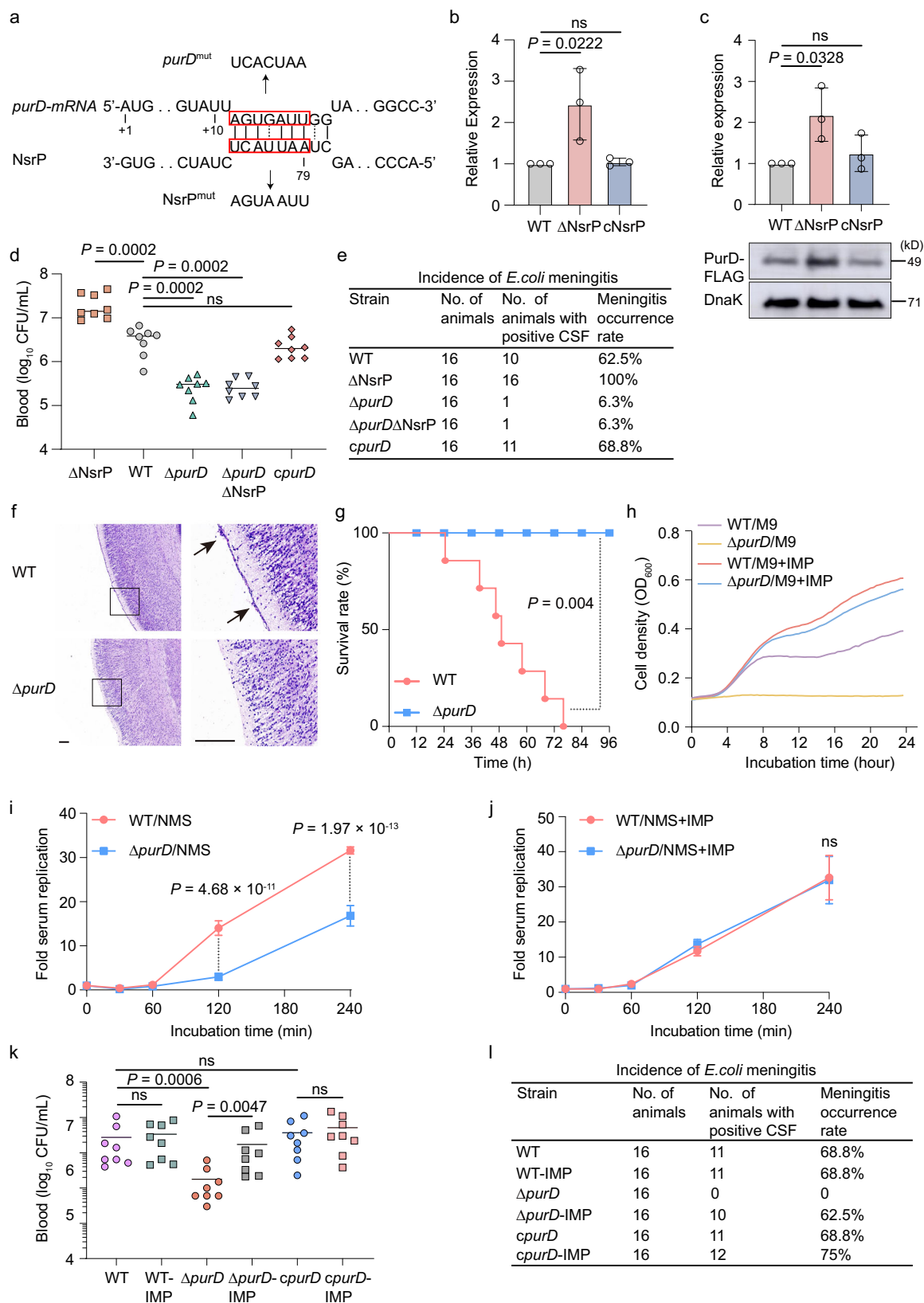
(**e**). **f** H&E staining of brain sections was performed 4 h after intravenous injection of 1×10^6 CFU of the WT or Δ NsrP strain. The right panels are higher-magnification images of the boxed regions, showing meningeal thickening and neutrophil infiltration (arrows). Scale bar, 100 μ m. The images shown are representative of three independent experiments. **g** Survival curves of 2- to 5-day-old rats subcutaneously injected with 1×10^5 CFU of the WT or Δ NsrP strain ($n = 16$ for each group). The number of living animals was recorded every 8 h. ns, nonsignificant. The two-tailed Mann–Whitney *U*-test (**d**), and the log-rank (Mantel–Cox) test (**g**) were applied.

Additionally, brain sections of the infected mice were examined by hematoxylin and eosin (H&E) staining. Compared with those in WT strain-infected mice, thickened meninges with neutrophil infiltration were observed in the mice infected with Δ NsrP (Fig. 1f), demonstrating that NsrP deletion leads to aggravated inflammation in the cerebral meninges. We next investigated the influence of NsrP on NMEC virulence by monitoring the survival of 2- to 5-day-old rats infected subcutaneously with WT or Δ NsrP NMEC²⁷. Survival curves showed that all the neonatal rats infected with the Δ NsrP strain died at 48 h post-infection, while only 50% of the neonatal rats infected with the WT

strain died at 48 h post-infection (Fig. 1g), suggesting that the mortality induced by the Δ NsrP strain was accelerated compared with that induced by the WT strain. These results demonstrated that NsrP inhibits bacterial survival in the blood and penetration of the BBB, resulting in a decrease in bacterial virulence.

NsrP inhibits NMEC virulence by repressing *purD* expression

In total, 387 putative target genes of NsrP were predicted in the genome of RS218 using TargetRNA3 (Supplementary Data 1). Among these potential target genes, *purD* may be a potential target of NsrP because



the predicted base-pairing domain was included in the *purD* mRNA near the initiation codon (Fig. 2a). The *purD* gene encodes a phosphoribosylamine-glycine ligase that has been identified by transposon insertion sequencing as an NMEC gene required for survival in human serum^{20,28}. qRT-PCR assays revealed that *purD* expression was significantly greater in the Δ NsrP strain than in the WT and cNsrP

strains, suggesting that NsrP negatively regulates *purD* expression (Fig. 2b). To determine the expression of PurD at the protein level, a chromosomally 3×FLAG C-terminal fusion construct of *purD* was generated. Western blotting was performed to quantify the levels of FLAG-tagged PurD in LB medium for the WT, Δ NsrP and cNsrP strains. The results showed that, compared with the WT and cNsrP strains, the

Fig. 2 | NsrP negatively regulates virulence by inhibiting *purD* expression. **a** The regions of base pairing between NsrP and *purD* as predicted by the TargetRNA3 with the probability threshold of 0.25 and *p*-value of 0.05. Point mutations to generate the disrupted alleles. **b** qRT-PCR analysis of *purD* in the NMEC WT, ΔNsrP, and cNsrP. **c** Western blot analysis and quantification of PurD-FLAG in the NMEC WT, ΔNsrP, and cNsrP. DnaK was used as the loading control. **d, e** Bacterial counts in the blood (CFU/mL, **d**) and meningitis development (**e**) were determined 4 h after intravenous injection of 1×10^6 CFU of the WT, ΔNsrP, Δ*purD*, ΔNsrPΔ*purD* or Δ*purD* complemented (*cpurD*) strain (*n* = 8 for each group in **d**). CSF culture positivity was defined as meningitis. **f** H&E staining of the brain sections was performed 4 h after intravenous injection of 1×10^6 CFU of the WT or Δ*purD*. The right panels are higher-magnification images of the boxed regions, showing meningeal thickening and

neutrophil infiltration (arrows). Scale bar, 100 μm. The images shown are representative of three independent experiments. **g** Survival curves of 2- to 5-day-old rats subcutaneously injected with 1×10^5 CFU of the WT or Δ*purD* (*n* = 16 for each group). The number of living animals was recorded every 8 h. **h** Growth curves of the WT and Δ*purD* in M9 medium with or without 40 mM IMP. **i, j** Replication of the WT and Δ*purD* in 60% NMS with (**j**) or without (**i**) 40 mM IMP. **k, l** Bacterial counts in the blood (CFU/mL, **k**) and meningitis development (**l**) were determined 4 h after intravenous injection of 1×10^6 CFU of the WT, Δ*purD*, or *cpurD* with or without IMP (*n* = 8 for each group in **k**). CSF culture positivity was defined as meningitis (**l**). ns nonsignificant. In **b, c, h–j**, data were presented as the means ± SDs (*n* = 3 independent experiments). One-way ANOVA (**b, c, i, j**), two-tailed Mann–Whitney *U*-test (**d, k**), log-rank (Mantel–Cox) test (**g**), and two-way ANOVA (**h**) were applied.

ΔNsrP strain exhibited increased PurD-FLAG production (Fig. 2c). These results demonstrate that NsrP inhibited PurD production.

To determine the effect of *purD* on NMEC pathogenicity, we performed HBMEC invasion assays and found that there was no significant difference in the bacterial capacity to invade HBMECs among the WT, Δ*purD* and Δ*purD* complemented (*cpurD*) strains (Supplementary Fig. 2a). A previous investigation established the limited availability of nucleotide precursors in blood^{23,29}. In addition, the inactivation of nucleotide biosynthesis genes in *Salmonella enterica* and *Bacillus anthracis* has been demonstrated to impede their growth in human serum²⁴. Therefore, we examined the impact of *purD* on the capacity of NMEC to elicit bacteremia and meningitis in a mouse model of experimental hematogenous meningitis. Compared with the WT strain, the Δ*purD* strain elicited a 12.4-fold lower level of bacteremia in mice, with bacterial loads of 6.46 ± 0.32 log CFU/ml for the WT strain and 5.38 ± 0.28 log CFU/ml of blood for the Δ*purD* strain (Fig. 2d). Similarly, the development of *E. coli* meningitis was markedly suppressed in Δ*purD*-infected mice compared to that in mice infected with the WT or *cpurD* strain (Fig. 2e). H&E staining of brain sections revealed thickened meninges with neutrophil infiltration in mice infected with WT, whereas no discernible histopathology was observed in the meninges of the animals infected with Δ*purD* (Fig. 2f). Survival curves showed that 50% of the neonatal rats infected with the WT strain died 48 h post-infection, whereas those infected with the Δ*purD* strain remained viable at the end of the observation period (96 h post-infection, Fig. 2g). Collectively, these results provide evidence that *purD* facilitates the survival and replication of NMEC within the murine bloodstream, which enhances bacterial penetration across the BBB and meningitis development.

Furthermore, we investigated whether NsrP regulates the virulence of NMEC via *purD*. Animal experiments showed that the double-mutant ΔNsrPΔ*purD* and Δ*purD* strains induced comparable levels of bacteremia in mice, with no significant difference in their capacity to cause meningitis development (Fig. 2d, e). Both strains exhibited significantly reduced virulence compared to the WT and ΔNsrP strains in infected mice (Fig. 2d, e). Additionally, the ΔNsrP strain induced significantly higher levels of bacteremia and an increased incidence of meningitis in mice compared to the WT strain (Fig. 2d, e), consistent with the results presented above (Fig. 1d, e). These findings suggest that the deletion of NsrP had no effect on NMEC virulence in the Δ*purD* background and that the regulatory effect of NsrP on the virulence of NMEC is mediated by *purD*.

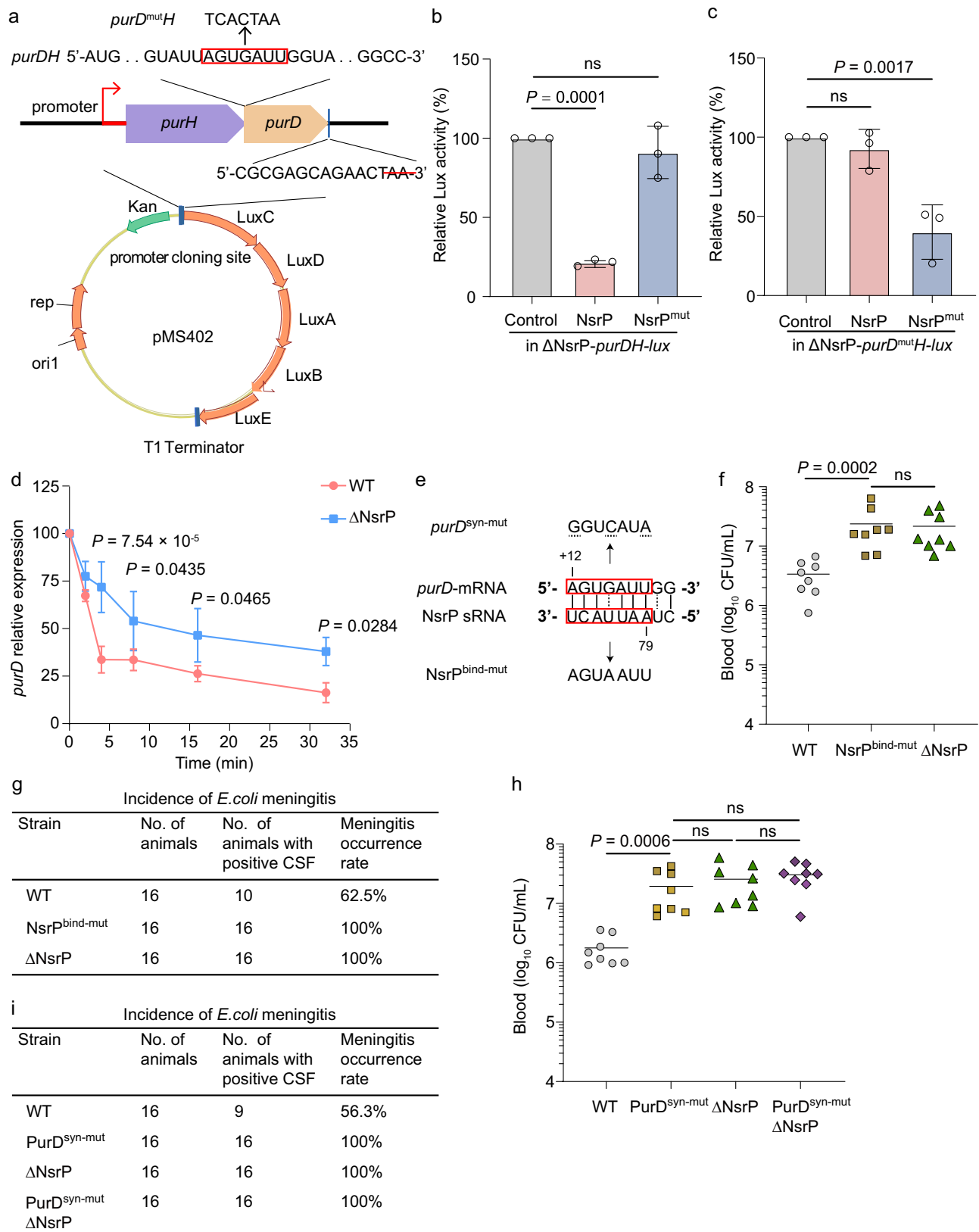
Bacterial growth curves demonstrated that, compared with the WT strain, the Δ*purD* strain exhibited a growth deficiency when cultured in the M9 medium (Fig. 2h), which is a minimal medium devoid of purines and their derivatives. However, when M9 medium was supplemented with 40 mM IMP, the growth of the Δ*purD* strain was similar to that of the WT strain (Fig. 2h). In addition, we showed that compared with the WT strain, the Δ*purD* strain exhibited a reduced capacity for growth in both normal mouse serum (NMS) and heat-inactivated normal mouse serum (HI-NMS) after 2 or 4 h of incubation

in vitro (Fig. 2i and Supplementary Fig. 2b). Conversely, the WT and Δ*purD* strains exhibited comparable growth rates in NMS and HI-NMS when supplemented with IMP (Fig. 2j and Supplementary Fig. 2c). Furthermore, animal experiments demonstrated that the intravenous injection of IMP enhanced the ability of the Δ*purD* but not the WT and *cpurD* strains to induce bacteremia and meningitis in mice (Fig. 2k, l). These findings suggest that the survival impairment observed for the Δ*purD* strain is attributable to the deficiency of purines in the bloodstream and the impairment of purine synthesis.

NsrP directly binds to *purD* mRNA

To test for a direct interaction between NsrP and *purD* mRNA in vitro, we performed an RNA electrophoretic mobility shift assay (REMSA) using in vitro-transcribed and purified NsrP and *purD* mRNA or the NsrP complementary strand as a positive control (NsrP+) (Supplementary Fig. 3a, b). NsrP-*purD* mRNA complexes were observed, and the band intensity increased as the NsrP concentration increased (Supplementary Fig. 3a), confirming the direct interaction between NsrP and *purD* mRNA in vitro.

IntaRNA analysis showed that NsrP may interact with the *purD* mRNA through nine-nucleotide base (CUAAUUAUCU) pairing beginning at nucleotide +12 in the *purD* mRNA (based on the ATG site) (Fig. 2a). The prediction of the secondary structure of NsrP sRNA via RNAfold revealed that this binding motif of NsrP is located in a loop structure (Supplementary Fig. 3c). To confirm that this motif is the key sequence of NsrP required for binding to *purD* mRNA, we performed REMSA using a mutated NsrP (NsrP^{mut}) (the motif AAUUAUCU was complementarily mutated to UUAUAUGA, which did not affect the secondary structure of NsrP), and a mutated *purD*^{mut} mRNA (the sequence AGUGAUU was complementarily mutated to UCACUAA) (Fig. 2a). No interaction was observed between the NsrP^{mut} sRNA and *purD* mRNA or between the NsrP sRNA and *purD*^{mut} mRNA (Supplementary Fig. 3d, e). However, REMSA showed a direct interaction between the NsrP^{mut} sRNA and *purD*^{mut} mRNA (Supplementary Fig. 3f). Moreover, we constructed a plasmid containing *purDH-lux* fusion (*purD* and *purH* are located in an operon³⁰) (Fig. 3a and Supplementary Fig. 3g), and introduced this plasmid into ΔNsrP, generating strain ΔNsrP-*purDH-lux*. We found a significant reduction in the luminescence intensity of the ΔNsrP-*purDH-lux* strain when NsrP was overexpressed (Fig. 3b). In contrast, overexpressing NsrP^{mut} with mutated binding motif did not influence the luminescence intensity (Figs. 2a, 3b). Furthermore, there was no significant difference in the luminescence intensity of the ΔNsrP-*purD*^{mut}-*H-lux* strain (the binding motif AGUGAUU of *purDH-lux* on the plasmid was complementarily mutated to UCACUAA) when NsrP was overexpressed, whereas a significant reduction in the luminescence intensity was observed when NsrP^{mut} was overexpressed in ΔNsrP-*purD*^{mut}-*H-lux* strain (Fig. 3a, c). In addition, northern blotting showed that there is no significant difference between the expression of NsrP and NsrP^{mut} (Supplementary Fig. 3h, i). Collectively, these data indicate that NsrP binds directly and specifically to the *purD* mRNA through the identified motif (AAUUAUCU).



To investigate whether NsrP influences the stability of *purD* mRNA, we performed a rifampicin transcription inhibition assay. The results showed that the *purD* mRNA was more stable in the Δ NsrP strain than in the WT strain (Fig. 3d), indicating that NsrP was detrimental to *purD* mRNA stability. Furthermore, we found that the expression of *purD* in the Δ hfq strain exhibited no significant difference compared with that in

the WT strain in rifampicin transcription inhibition assay (Supplementary Fig. 3j). In contrast, the expression of *purD* was significantly increased in the Δ hfq Δ NsrP strain compared with that in the Δ hfq strain (Supplementary Fig. 3k). These results suggest that NsrP-*purD* base pairing promotes *purD* mRNA degradation in an Hfq-independent way and thus decreases PurD expression.

Fig. 3 | NsrP binds to *purD* mRNA and negatively regulates its stability in NMEC. **a** Schematic of the structure of *purDH-lux*. The region of the *purDH* promoter and the expected full-length *purDH* without termination codon were cloned and inserted into pMS402 to construct a *purDH-lux* fusion. Point mutations to generate the disrupted alleles in the *purD^{mut}H* transcript are indicated. **b, c** Quantification of the PurD (**b**) or PurD^{mut} (**c**) protein expression level in the ΔNsrP-*purDH-lux* strain (**b**) or ΔNsrP-*purD^{mut}H-lux* strain (**c**) by measurement of luminescence. The ΔNsrP-*purDH-lux* and ΔNsrP-*purD^{mut}H-lux* strains were transformed with the expression construct pNM12 (Control), or pNM12 encoding NsrP or NsrP^{mut}. **d** qRT-PCR analysis

of *purD* expression in rifampicin-treated the WT and ΔNsrP strains. **e** Graphical presentation of proposed interaction of NsrP sRNA with the *purD* mRNA, and of base-pair changes to generate NsrP^{bind-mut} and PurD^{syn-mut}. **f–i** Bacterial counts in the blood (CFU/mL, **f, h**) and meningitis development (**g, i**) were determined 4 h after intravenous injection of 1×10^6 CFU of the WT, NsrP^{bind-mut}, and ΔNsrP strains (**f, g**) or WT, PurD^{syn-mut}, ΔNsrP, and PurD^{syn-mut}ΔNsrP strains (**h, i**) ($n = 8$ for each group in **f, h**). CSF culture positivity was defined as meningitis. In **b–d**, data were presented as the means \pm SDs ($n = 3$ independent experiments). ns nonsignificant. One-way ANOVA (**b–d**), and two-tailed Mann–Whitney *U*-test (**f, h**) were applied.

To further identify the contribution of the NsrP binding motif to NMEC virulence in vivo, we mutated the NsrP binding motif (AAUUACU to UUAAGA) on the chromosome of WT, generating strain NsrP^{bind-mut}. We also mutated the binding motif on *purD* by synonymous mutation (AGUGAUU to GGUCAUA) on the chromosome of WT, generating strain PurD^{syn-mut} (Fig. 3e). We found that the levels of bacteremia and the incidence of meningitis elicited by the NsrP^{bind-mut} and PurD^{syn-mut} strains in mice were significantly higher than that in WT-infected mice, which exhibited no significant difference from that in ΔNsrP-infected mice (Fig. 3f–i). Moreover, we further deleted NsrP in strain PurD^{syn-mut} (generating strain PurD^{syn-mut}ΔNsrP), and found that the levels of bacteremia and the incidence of meningitis in mice infected by PurD^{syn-mut}ΔNsrP exhibited no significant difference from that in mice infected by PurD^{syn-mut} (Fig. 3h, i). This finding suggests that the regulatory effect of NsrP on the virulence of NMEC is mediated by its binding to *purD* mRNA.

NMEC senses low leucine levels in the blood to suppress NsrP expression

qRT-PCR analysis of WT NMEC recovered from the blood of mice infected via tail vein injection showed that NsrP expression decreased compared with that of WT NMEC in LB medium (Fig. 4a). To investigate the potential factors regulating NsrP expression, an analysis of the NsrP promoter region was conducted using the online promoter prediction tool BProm. This analysis confirmed the presence of an Lrp-binding site within the NsrP promoter region (Fig. 4b). qRT-PCR analysis revealed a significant decrease in NsrP expression in the ΔLrp strain compared with that in the WT strain when cultured in LB medium (Fig. 4c), indicating that Lrp positively regulates NsrP expression.

To investigate whether Lrp directly binds to the NsrP promoter, we performed a surface plasmon resonance (SPR) assay to monitor the real-time binding of Lrp to the NsrP promoter. The result showed that the purified Lrp (but not BSA) binds to the promoter of NsrP in a dose-dependent manner (Fig. 4d and Supplementary Fig. 4a). Consistently, chromatin immunoprecipitation-qPCR (ChIP-qPCR) analysis revealed 9.51-fold greater enrichment of the NsrP promoter region in Lrp-ChIP samples than in the mock-ChIP samples (Fig. 4e). In contrast, the fold enrichment of *rpoS* did not significantly differ between these two samples (Fig. 4e). These results indicate that Lrp specifically binds to the NsrP promoter region both in vitro and in vivo.

E. coli Lrp was initially identified as a leucine-responsive regulatory protein, but subsequent research has also indicated its responsiveness to various other small effector molecules, including alanine, methionine, threonine, lysine, histidine, and isoleucine³¹. Thus, we carried out qRT-PCR to analyze NsrP expression in response to each of these amino acids. Mid-logarithmic phase WT strain incubated in LB medium was collected and reincubated in M9 minimal medium supplemented with different concentrations of these amino acids for 30 min. The qRT-PCR results revealed that NsrP expression decreased at a low leucine concentration (0.1 mM), which mimics conditions found in human blood³², compared to its expression at a high leucine concentration (5 mM). Conversely, the expression of NsrP did not significantly change in response to the other amino acids (Fig. 4f and Supplementary Fig. 4b). Similarly, northern blot analysis also revealed a decrease in NsrP expression in the WT strain under conditions of low

leucine levels, suggesting that NsrP expression is repressed by low leucine levels (Fig. 4g). Furthermore, we showed that leucine levels no longer regulate NsrP expression in the strains ΔLrp and NsrP^{pro-mut} (with Lrp binding site on the promoter of NsrP was deleted from the genome) (Fig. 4b, h, i). These findings provide evidence that NMEC senses low leucine levels through Lrp to suppress NsrP expression by binding to its promoter directly.

NMEC promotes *purD* expression in mouse blood by sensing low leucine levels in an NsrP-dependent manner

As NsrP expression was repressed at a low level of leucine and NsrP served as a negative regulator of *purD* expression, our subsequent investigation focused on the impact of leucine on *purD* expression. qRT-PCR was performed on mid-logarithmic phase WT strains reincubated in M9 minimal medium supplemented with different concentrations of leucine (0.1 or 5 mM) for 30 min. The results revealed a significant increase in *purD* expression under low-leucine conditions (Fig. 5a). This finding is consistent with the observed upregulation of *purD* expression in mouse blood, which is a low-leucine environment compared with LB medium (Fig. 5b). To determine the impact of leucine on PurD expression at the protein level, a 3×FLAG-PurD WT strain was incubated in the same conditions. Western blotting results showed that PurD-FLAG production was significantly induced by low leucine levels (Fig. 5c). In contrast, in the ΔLrp, ΔNsrP, and NsrP^{pro-mut} strains, the regulation of *purD* expression by leucine was no longer observed (Fig. 5d–f). These results demonstrated that NMEC senses low leucine levels in the blood to increase *purD* expression in an Lrp- and NsrP-dependent manner.

In summary, our study demonstrated that NMEC can sense low leucine levels in the bloodstream, leading to a decrease in NsrP expression, which in turn increases *purD* expression in an Lrp-dependent manner. This phenomenon increases NMEC survival in the host bloodstream. These findings suggest that a low leucine level is beneficial for NMEC survival in the bloodstream, which is consistent with the finding that NsrP mutation promotes NMEC pathogenicity.

purD did not affect the intestinal colonization of NMEC

NMEC infections arise due to the colonization of the neonatal gastrointestinal tract by maternally derived NMEC at or soon after birth, followed by transcytosis through enterocytes into the bloodstream and ultimately the development of meningitis^{6,7}. In addition, the gut can serve as a reservoir for the recurrence of NMEC infection³³. To investigate the impact of *purD* on the colonization of NMEC in the intestine, we performed qRT-PCR to determine the expression of NsrP and *purD* in the rat intestine. The results showed that NsrP and *purD* expression in the WT strain that colonized the small intestine did not significantly differ from that in the LB medium (Supplementary Fig. 5a). Moreover, bacterial colonization in the small intestine also did not significantly differ among the NMEC WT, Δ*purD*, and *cpurD* strains (Supplementary Fig. 5b), suggesting that *purD* was not necessary for NMEC intestinal colonization. Previous research has demonstrated that the small intestine of infants is abundant in purines and amino acids, including leucine^{34–37}. Therefore, the small intestine serves as a niche for NMEC infection that does not require upregulation of the de novo purine synthesis pathway.

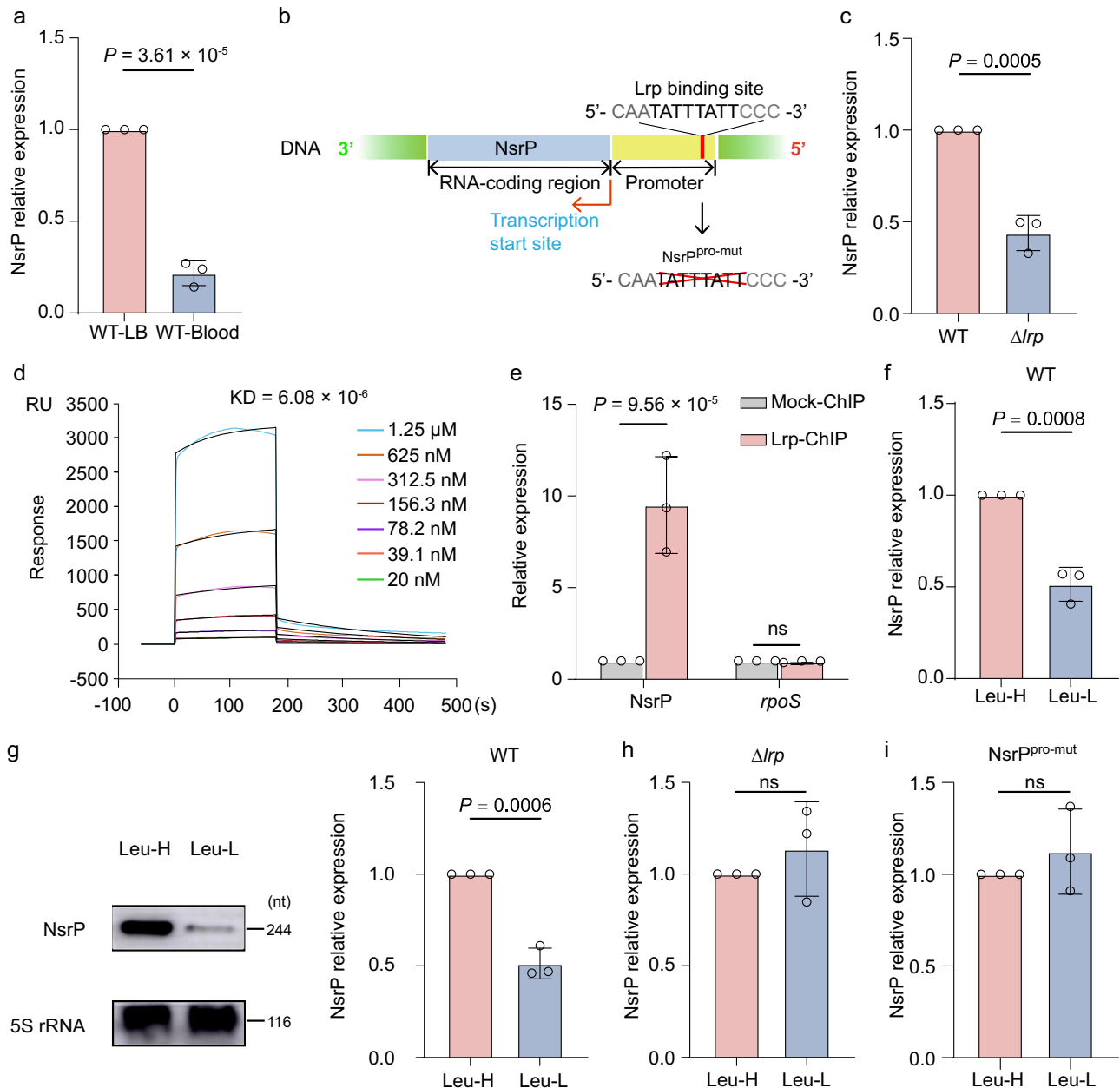


Fig. 4 | Low leucine levels repressed NsrP expression via Lrp. **a** qRT-PCR analysis of NsrP expression in the NMEC WT strain in LB medium and mouse blood. **b** The NsrP promoter region and the potential binding site of Lrp were predicted by the BProm program (SoftBerry). **c** qRT-PCR analysis of the NsrP expression in WT and Δlrp . **d** Biacore SPR kinetic analyses of Lrp binding to the promoter of NsrP. **e** Fold enrichment of the NsrP promoter in the Lrp-ChIP samples compared with that in the mock-ChIP samples. **f** qRT-PCR analysis of the NsrP expression in WT NMEC in

M9 medium supplemented with 0.1 mM leucine (Leu-L) or 5 mM leucine (Leu-H). **g** Northern blotting of NsrP sRNA in WT NMEC in M9 medium supplemented with 0.1 or 5 mM leucine. 5S rRNA was used as the loading control. **h**, **i** qRT-PCR analysis of the NsrP expression in the Δlrp (**h**) and NsrP^{pro-mut} (**i**) strain in M9 medium supplemented with 0.1 or 5 mM leucine. In **a**, **c**, **e**–**i**, data were presented as the means \pm SDs ($n = 3$ independent experiments). ns nonsignificant. Two-tailed unpaired Student's *t*-test (**a**, **c**, **f**–**i**) and two-way ANOVA (**e**) were applied.

Intravenous administration of leucine reduced NMEC virulence in mice by blocking the Lrp-NsrP-PurD regulatory pathway

The above results showed that NMEC senses low levels of leucine in the blood to increase the expression of *purD* by repressing NsrP expression, which results in significantly increased NMEC pathogenicity. Therefore, the leucine level may be a potential factor for the treatment of NMEC infection. Thus, mice infected by NMEC WT were treated with leucine through tail vein injection at 0.5 h post-infection to determine the effect of leucine on NMEC pathogenicity. The results showed that leucine treatment resulted in significantly increased or decreased bacterial expression of NsrP and *purD* in vivo, respectively, compared to control mice (WT-infected mice receiving PBS) (Fig. 6a, b). Moreover, leucine-

treated mice exhibited significantly decreased levels of bacteremia and inhibited development of meningitis compared to control mice (Fig. 6c, d). Additionally, the leucine-treated mice exhibited less thickened meninges with neutrophil infiltration than did the control mice (Fig. 6e). Conversely, there was no significant difference in bacteremia levels or the development of meningitis between leucine-treated mice and control mice when they are infected with strain Δ NsrP, Δ purD, NsrP^{pro-mut}, NsrP^{bind-mut}, or PurD^{syn-mut} (Fig. 6f–k). Collectively, these data indicate leucine is able to reduce the pathogenicity of NMEC by blocking the Lrp-NsrP-PurD regulatory pathway.

To investigate whether the administration of leucine, which targets the Lrp-NsrP-PurD regulatory pathway, could be a potential

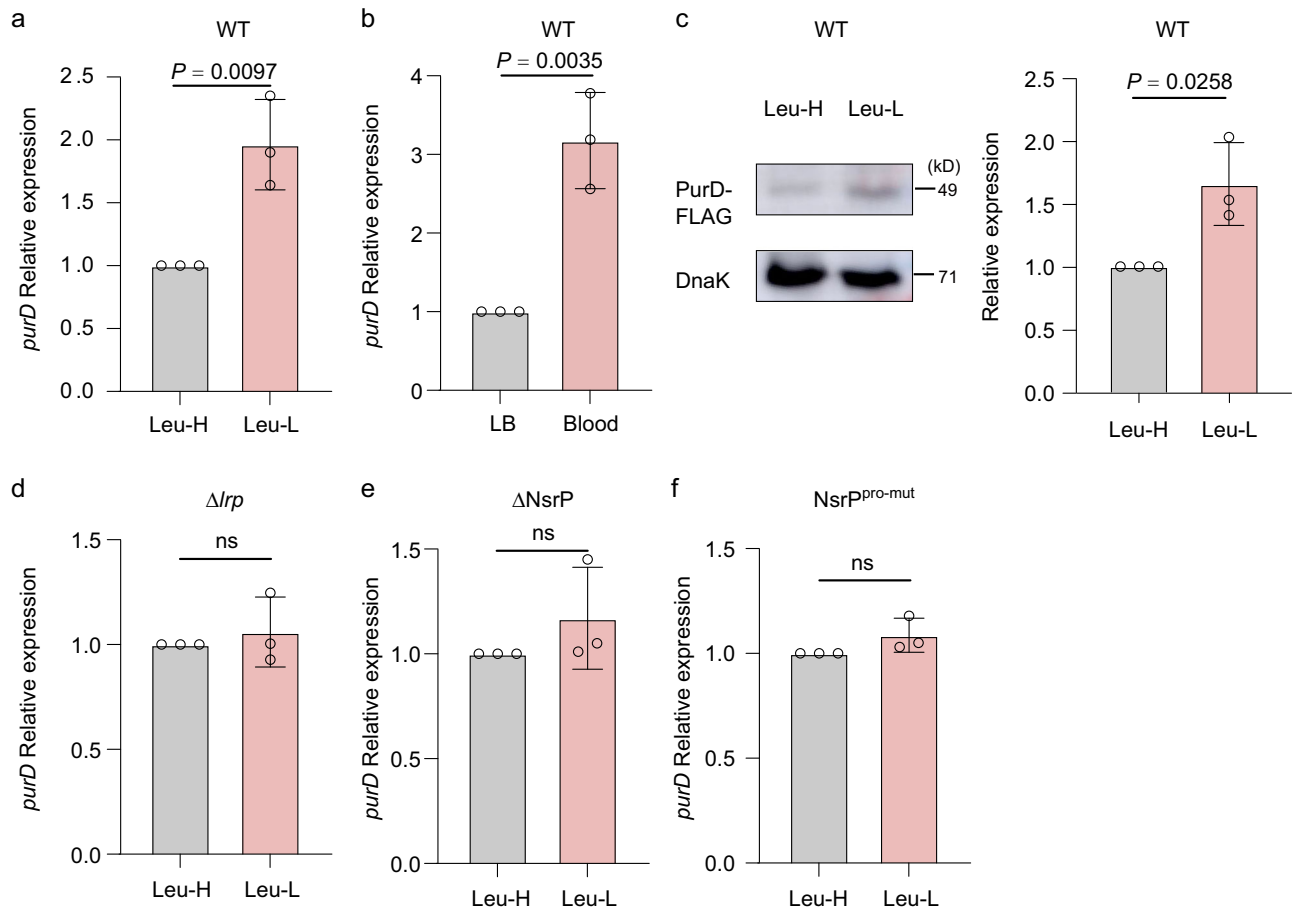


Fig. 5 | Low leucine levels induced *purD* expression via NsrP. **a** qRT-PCR analysis of the *purD* expression in the NMEC WT strain in M9 medium supplemented with 0.1 or 5 mM leucine. **b** qRT-PCR analysis of the *purD* expression in WT NMEC in LB medium or mouse blood. **c** Western blot analysis and quantification of PurD-FLAG in WT NMEC in M9 medium supplemented with 0.1 or 5 mM leucine. DnaK was used

as the loading control. **d–f** qRT-PCR analysis of the *purD* expression in the Δlrp (**d**), $\Delta NsrP$ (**e**), and $NsrP^{pro-mut}$ (**f**) strain in M9 medium supplemented with 0.1 or 5 mM leucine. In **a–f**, data were presented as the means \pm SDs ($n = 3$ independent experiments). ns, nonsignificant. Two-tailed unpaired Student's *t*-test was applied.

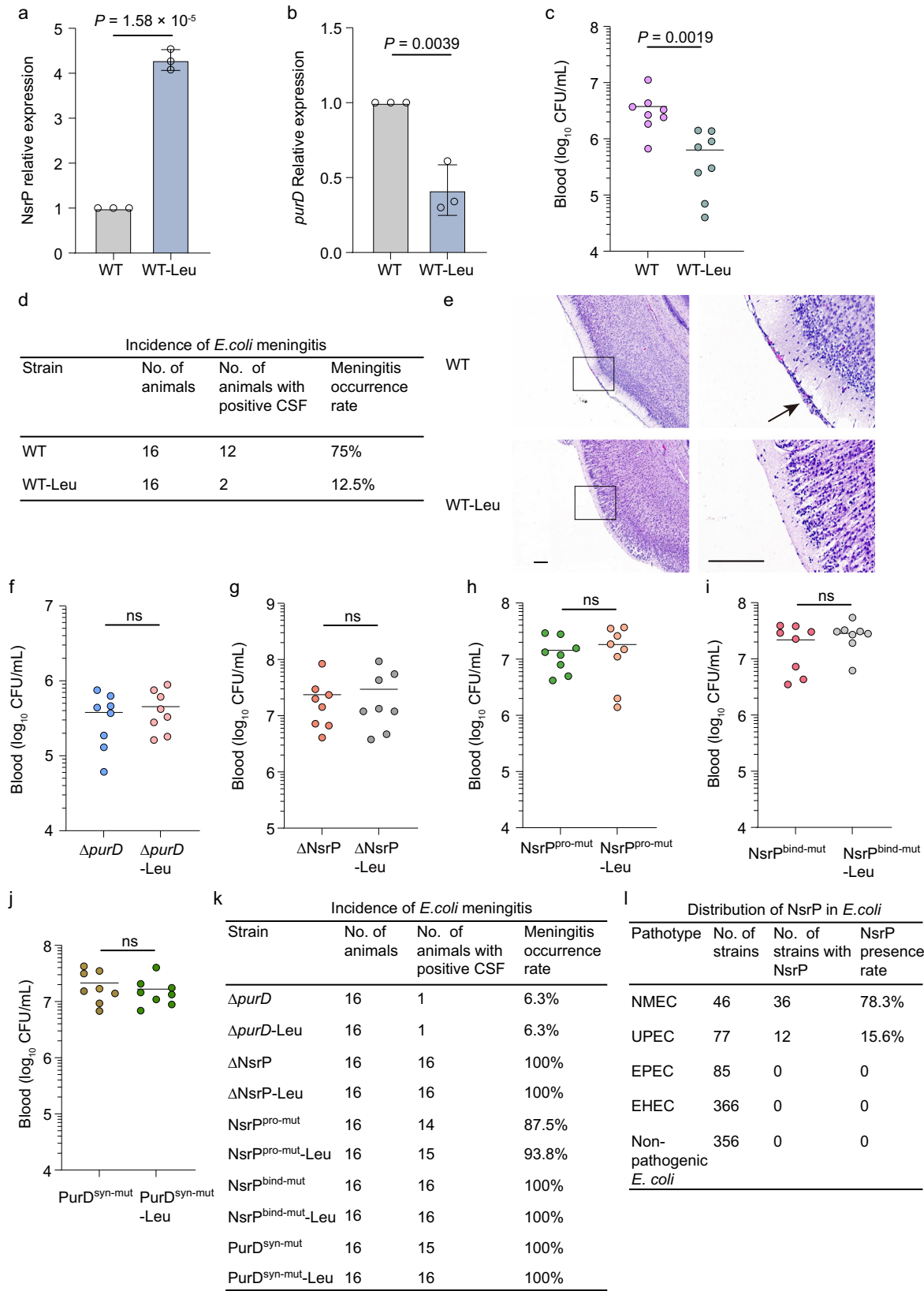
strategy for the treatment of *E. coli* bacteremia and meningitis, we analyzed the distribution of NsrP in *E. coli* by performing a comparative genomics analysis using 930 publicly available complete *E. coli* genomes. The genomes of the strains included 46 NMEC strains, 77 uropathogenic *E. coli* (UPEC) strains, 85 enteropathogenic *E. coli* (EPEC) strains, 366 EHEC strains, and 356 nonpathogenic *E. coli* strains. The results showed that NsrP was present in the majority of the NMEC strains (36/46, 78.3%) and in a few UPEC strains (12/77, 15.6%) whose serotypes were O1 and O18 (Fig. 6l, Supplementary Data 2). In contrast, NsrP was absent in the EHEC, EPEC, and nonpathogenic *E. coli* strains (Fig. 6l). Furthermore, among the 34 NMEC strains that possessed a K1 capsule (34/46, 73.9%, defined as *E. coli* K1⁺), 29 harbored NsrP (29/34, 85.3% in *E. coli* K1⁺), suggesting that NsrP is widely present in *E. coli* K1⁺ strains. These results indicate that NsrP is widely distributed in NMEC but not in nonpathogenic *E. coli* or other pathotypes of *E. coli*. Thus, the administration of leucine to target the Lrp-NsrP-PurD regulatory pathway is a potential strategy for the prevention and treatment of *E. coli* bacteremia and meningitis.

Discussion

To survive and thrive in an often hostile environment, bacteria must monitor their surroundings and adjust their gene expression and physiology accordingly. This is especially important for pathogenic bacteria, which continuously interact with the host during an infection³⁸. In this study, we elucidated an NsrP-mediated regulatory signal transduction pathway employed by NMEC to sense low leucine

levels in the host bloodstream. This perception leads to the augmentation of bacterial purine biosynthesis, thereby facilitating the progression of bacteremia and meningitis. Specifically, NsrP destabilizes the mRNA of the purine biosynthesis-related gene *purD*, resulting in the downregulation of *purD* expression. A low leucine level in the blood decreases NsrP expression via Lrp, which ultimately increases *purD* expression, resulting in enhanced purine biosynthesis. This mechanism significantly contributes to NMEC proliferation within the bloodstream, consequently inducing bacteremia and bacterial meningitis (Fig. 7).

In bacterial pathogens, sRNAs can directly influence bacterial pathogenicity by regulating the expression of virulence factors. For example, in EHEC under microaerobic conditions, the sRNA DicF activates translation of *pchA*, which subsequently activates the transcription of *ler* resulting in the enhanced expression of genes within the LEE pathogenicity island¹³. Additionally, the sRNAs GlmY and GlmZ of EHEC repress the expression of *espADB* encoded by LEE4 and the transcripts from LEE5³⁹. In hypervirulent *Klebsiella pneumoniae*, the sRNA ArcZ regulates many hypermucoviscosity-related genes, causing the overproduction of the hypermucoviscous capsule, which is crucial for the hyper-virulence⁴⁰. This direct regulation of virulence genes by sRNAs enables pathogens to efficiently thrive within the host, offering a rapid response mechanism with minimal energy expenditure. However, sRNAs can also indirectly influence bacterial pathogenicity by modulating physiological activities such as adaptation to environmental stresses. For example, iron scarcity and oxidative stress are



common challenges pathogens face within the host. In *Pseudomonas aeruginosa*, the sRNA PrrH, regulates genes involved in pyochelin biosynthesis, enabling the pathogen to scavenge iron from human proteins like lactoferrin and transferrin in the form of Fe^{3+} ⁴¹. In *Salmonella Typhimurium*, the sRNAs CyaR, MicA, and OxyS have been identified as regulators of *ompX*, a gene involved in responses to

oxidative stress⁴². Additionally, in *P. aeruginosa*, the sRNA SicX regulates anaerobic ubiquinone biosynthesis, facilitating the transition between chronic and acute infections⁴³. Whether through direct regulation of virulence factors or modulation of bacterial metabolic responses to environmental stresses, these mechanisms are crucial for pathogen colonization and survival within the host. In our study, we

Fig. 6 | Administration of leucine attenuates NMEC virulence. **a, b** qRT-PCR analysis of the *NsrP* (**a**) and *purD* (**b**) expression in mouse blood were determined 4 h after intravenous injection of 1×10^6 CFU of the NMEC with the administration of leucine or PBS. **(c, d, f–k)** Bacterial counts in the blood (CFU/mL, **c, f–j**) and meningitis development (**d, k**) were determined 4 h after intravenous injection of 1×10^6 CFU of the WT (**c**), $\Delta purD$ (**f**), $\Delta NsrP$ (**g**), $NsrP^{pro-mut}$ (**h**), $NsrP^{bind-mut}$ (**i**), and $PurD^{syn-mut}$ (**j**) strains with the administration of leucine or PBS at 0.5 h post-infection ($n = 8$ for each group). CSF culture positivity was defined as meningitis (**d, k**). **e** H&E staining of the brain sections was performed 4 h after intravenous injection of

1×10^6 CFU of the WT strain and of leucine or PBS at 0.5 h post-infection. The right panels are higher-magnification images of the boxed regions, showing meningeal thickening and neutrophil infiltration (arrows). Scale bar, 100 μ m. The images shown are representative of three independent experiments. **l** The distribution of *NsrP* in 930 publicly available complete *E. coli* genomes. In **a, b**, data were presented as the means \pm SDs ($n = 3$ independent experiments). ns nonsignificant. Two-tailed unpaired Student's *t*-test (**a, b**) and two-tailed Mann–Whitney *U*-test (**c, f–j**) were applied.

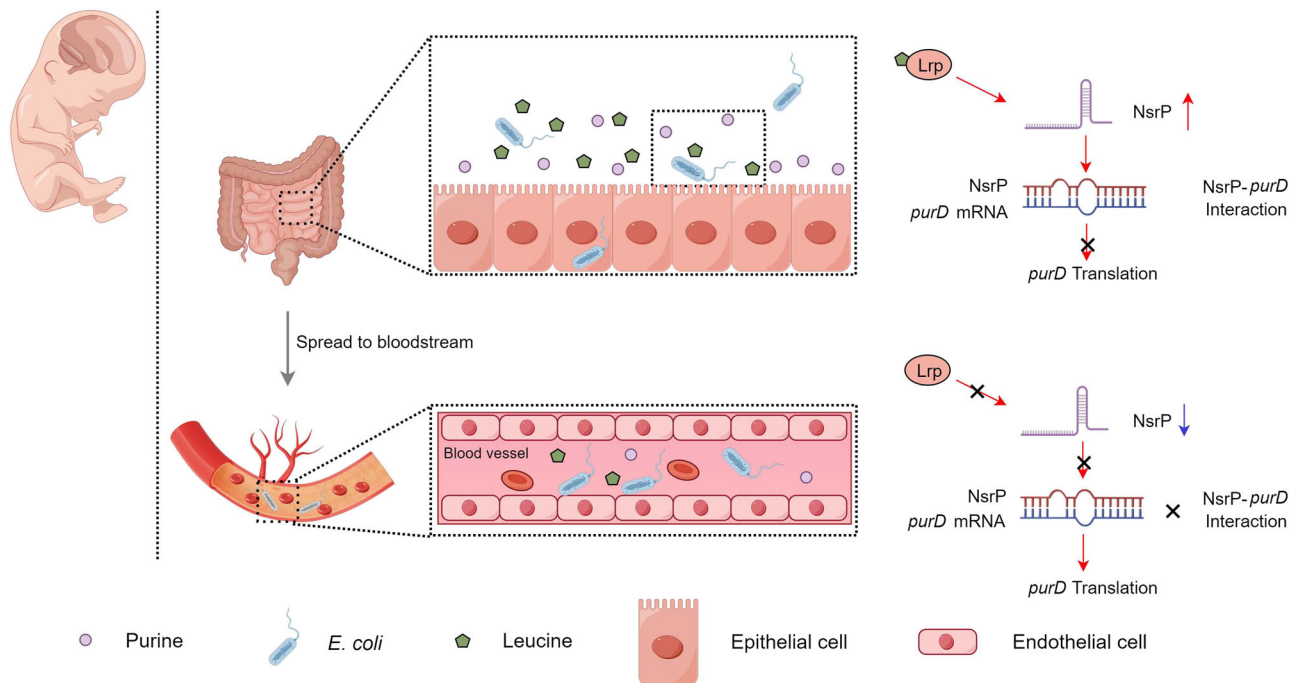


Fig. 7 | Model of purine synthesis regulation by NsrP in NMEC in response to leucine. (By Figdraw). In response to low leucine levels in the blood, NMEC downregulates the expression of *NsrP* in an Lrp-dependent manner. This promotes bacterial de novo purine biosynthesis, resulting in enhanced bacterial pathogenicity in the host.

identified an sRNA-mediated adaptive mechanism that helps NMEC respond to purine-limited environments in the host bloodstream, highlighting the essential role of sRNAs in facilitating bacterial survival under nutrient-restricted conditions.

The horizontal acquisition of certain genes can drastically alter the fitness of a bacterium, allowing it to utilize additional substrates and thrive in otherwise toxic environments^{44–46}. Numerous key *E. coli* pathogenicity genes have been identified by horizontal gene transfer, such as the locus of enterocyte effacement (LEE) and genomic O island 122 in EHEC⁴⁷. *NsrP* is a horizontally acquired sRNA that mediates the repression of *purD* expression in response to the leucine level. The scarcity of purines in blood, a nutrient-limiting condition, plays an important role in suppressing bacterial growth in blood²⁴. NMEC increases its purine synthesis in response to low leucine levels in the blood via the Lrp-NsrP-PurD signal transduction pathway, which is beneficial for NMEC survival and replication. In contrast, the small intestine of infants is abundant in purines since human milk contains considerable amounts of nucleotides that are digested in the small intestine³⁶. Moreover, the majority of dietary proteins are fully degraded in the small intestine, which makes this portion of the gastrointestinal tract abundant in amino acids, including leucine^{33,37}. Thus, we speculate that in the intestinal environment, NMEC does not need to upregulate the expression of purine synthesis genes (Supplementary Fig. 5a, b), enabling it to precisely regulate its energy consumption during infection (Fig. 7).

E. coli Lrp is a nucleoid-associated protein involved in the transcriptional regulation of numerous genes. Leucine is recognized as the

primary effector of Lrp, significantly modulating its regulatory activity by either enhancing or inhibiting its effects⁴⁸. Additionally, recent studies have shown that Lrp also responds to other amino acids, including alanine, methionine, isoleucine, lysine, histidine, and threonine³¹. For example, in addition to the canonical Lrp-leucine regulon in *E. coli*, the next most well-characterized group is the Lrp-alanine regulon, which includes genes involved in alanine export and metabolism⁴⁹. However, alanine regulates only a small subset of the Lrp regulon compared to leucine⁵⁰. This highlights leucine's unique ability to broadly influence Lrp-regulated gene networks compared to other effectors, although the underlying mechanism remains unclear. Previous studies have shown that leucine promotes the dissociation of the Lrp hexadecamer into leucine-bound octamers with altered DNA-binding affinity⁵¹. Based on this, we speculate that Lrp's ability to activate the expression of *NsrP* in response to leucine, rather than other amino acids, may be due to the specific oligomeric state induced by leucine. This hypothesis warrants further investigation in future studies.

Among clinical isolates, *E. coli* K1⁺ is predominant among isolates from neonatal *E. coli* meningitis and possesses a limited diversity of O-serotypes, dominated by O18, O1, O7, O16, and O45⁴. We found that *NsrP* is predominant in O18:K1 and O1:K1 strains, which are the dominant serotypes that cause neonatal meningitis in many countries^{52,53}. The strategy for treating NMEC infection usually involves the use of antibiotics⁵⁴. However, antibiotic treatment changes the composition of the gut microbiota, resulting in a negative impact on host health⁵⁵. Moreover, the widespread use of antibiotics has increased the

antibiotic resistance of many pathogenic bacteria, making treatment more challenging⁵⁶. Leucine is an essential amino acid that cannot be synthesized within the body and has been found to be, along with isoleucine and valine (the three components of branched-chain amino acids, BCAA), an effective pharmacological nutrient in several diseases⁵⁷. For instance, BCAA administration has been applied in septic patients to improve their nutritional status and outcomes⁵⁸. BCAA administration is also recommended for the treatment of liver failure due to their effect on the detoxification of ammonia to glutamine and their decreased concentration in patients with liver cirrhosis⁵⁹. Moreover, leucine supplementation has been proven as a nutritional treatment for sarcopenia due to its anabolic effects on cell signaling and protein synthesis in muscle in clinical trials^{60–62}. Therefore, leucine administration targeting the Lrp-NsrP-PurD signal transduction pathway is a potential strategy for the prevention and treatment of *E. coli* bacteremia and meningitis. In addition, NsrP is absent in other *E. coli* strains, suggesting that intravenous administration of leucine may have a minor effect compared to that of antibiotic treatment on the gut microbial composition and diversity.

Methods

Ethics statement

All animal experiments were conducted in compliance with the guidelines outlined in the Guide for the Care and Use of Laboratory Animals. All animal studies were conducted according to protocols approved by the Institutional Animal Care Committee of Nankai University (Tianjin, China) and were performed under protocol no. IACUC 2016030502.

Bacterial strains, plasmids, and growth conditions

All the *E. coli* K1 strains used in this study were derived from a clinical isolate RS218 (serotype O18:K1:H7), which was isolated from the CSF of a newborn infant with meningitis⁶³. Plasmids, strains, and primers are listed in Supplementary Tables 1, 2. The mutants were generated using the λ -red recombination system to substitute the target genes with the chloramphenicol or kanamycin resistance genes in plasmid pKD3 or pKD4⁶⁴. The complemented strains were constructed by cloning the open reading frame and promoter region of corresponding genes into a plasmid, pACYC184. For purification of Lrp-6 \times His protein, *lrp* was cloned into the pET-28a expression vector and transferred into *E. coli* BL21 (DE3). For ChIP-qPCR, *lrp* was tagged with 3 \times FLAG, cloned into pTRC99A and transferred into Δ lrp. All the resulting clones were verified by PCR amplification and DNA sequencing. The test strains were grown in LB broth at 37 °C with required antibiotics (ampicillin, 100 μ g/mL; chloramphenicol, 25 μ g/mL; kanamycin, and 50 μ g/mL).

Small RNA candidate prediction

RNA sequencing data (SRA: PRJNA680436) were initially mapped to the genome RS218 (GenBank accession number: CP007149.1) using Bowtie2. Rockhopper software was then employed to identify intergenic and Cis-natural antisense transcripts⁶⁵. A BlastX search against the non-redundant NCBI database was performed to annotate these transcripts. Transcripts that remained unannotated were considered potential candidates for noncoding sRNA⁶⁶.

5' and 3' RACE assay

5' and 3' RACE assay were carried out using 5' and 3' RACE System for Rapid Amplification of cDNA Ends kits (Invitrogen, CA, USA) according to the manufacturer's instructions. In brief, for 5' RACE, the first strand of cDNA is synthesized from total RNA using a gene-specific primer. Following purification, cDNA was Oligo (dC)-tailed, and PCR was performed using an Abridged Anchor Primer and a nested gene-specific primer. The products were cloned into pEASY-T1 (TransGen, Beijing, China; CT111) and sequenced. For 3' RACE, the total RNA was applied for 3'-poly (A) tailing before reverse transcription using the adapter

primer. The gene-specific primer and the universal amplification primer that targets the adapter region were used for amplification. The products were cloned into pEASY-T1 and sequenced. The oligonucleotides used in these assays are listed in Supplementary Table 2.

RNA extraction and quantitative PCR (qPCR)

For NMEC collected from the blood of NMEC-infected mice, the specimens were collected as follows. 18-day-old BALB/c mice received 1×10^6 CFU of NMEC WT or mutant strains in the logarithmic phase of growth via the tail vein. Four hours later, blood specimens were collected. For NMEC collected from the small intestine, 2- to 5-day-old Sprague-Dawley rat pups were orally infected by pipette feeding of 20 μ L PBS containing 2×10^6 CFU of NMEC WT or mutant strains in the logarithmic phase of growth. Small intestine specimens were collected following the contents were removed after 24 h infection. For the effect of leucine levels on NMEC, mid-logarithmic phase NMEC WT or mutant strains incubated in LB medium were collected and reincubated in M9 minimal medium (1 \times M9 salts, 2 mM MgSO₄, 0.1 mM CaCl₂, 0.4% glucose) supplemented with 0.1 or 5 mM leucine for 30 min. For the effect of Hfq protein on the stability of NsrP and degradation of *purD* mRNA, LB-cultured NMEC and Δ hfq strains in the logarithmic phase of growth were incubated with 100 μ g/mL of rifampicin for 0, 2, 4, 8, 16, 32 min. The specimens above were collected by centrifugation at 5000 \times g for 5 min.

The total RNA was extracted using a TRIzol reagent (Invitrogen, USA). RNA was treated with DNase I at 37 °C for 30 min, and the successful removal of DNA contamination was verified by PCR. The quality and quantity of RNA were determined by NanoDrop spectrophotometer (Thermo Fisher, USA). cDNA synthesis was performed by PrimeScript RT reagent Kit (Takara, USA, RR037A). qRT-PCR was performed using SYBR green PCR master mix (Applied Biosystems, 4367659) on QuantStudio 5 (Applied Biosystems, CA, USA). The relative mRNA expression level was analyzed using the $\Delta\Delta$ Ct method after normalizing to the Ct of the *rpoA*¹³. Each experiment was performed in triplicate.

In vitro transcription and RNA-RNA EMSA (REMSA)

The DNA templates were transcribed into NsrP, NsrP+ (positive control), NsrP^{mut} sRNA, *purD*, and *purD*^{mut} mRNA using the T7 High Efficiency Transcription Kit (TransGen, Beijing, China, JT101). RNA was purified by MagicPure[®] RNA Beads (TransGen, Beijing, China, EC501) and then checked in an 8% Tris-Acr-urea gel. REMSA was performed with NsrP, NsrP^{mut} sRNA (0, 10, 20, and 30 μ M) and *purD*, *purD*^{mut} mRNA or NsrP+ (positive control, 10 μ M) in REMSA binding buffer containing 10 mM HEPES [pH 7.3], 20 mM KCl, 2.4 mM MgCl₂, and 2.4 mM DTT. Reactions were incubated for 2–3 min at 85 °C and then at 37 °C for 45 min. The samples were separated by 8% native polyacrylamide gels and stained with SYBR Gold Nucleic Acid Gel Stain (Invitrogen, CA, USA, S11494) for 10 min, then imaged using SuperSignal west pico chemiluminescent substrate (Thermo). ImageJ software was used to measure band intensities.

Purification of Lrp protein and surface plasmon resonance (SPR)

The *lrp* sequence from NMEC RS218 genomic DNA was cloned into the pET-28a to obtain the pET-Lrp plasmid. Lrp-6 \times His protein was expressed in *E. coli* BL21 (DE3) containing pET-Lrp and purified using HiTrap Ni²⁺-chelating column. The concentration of Lrp was determined by the Bradford method⁶⁷. The PCR fragment of the NsrP promoter (NsrP-pro) were amplified with the 5'-biotinylated primers and purified using a SPAReasy Gel DNA Extraction Kit (Sparkjade, Shandong, China, AE0101). The interactions between 5'-biotinylated NsrP promoter DNA and Lrp (DNA-binding protein, ~20 kDa) or BSA (fatty acid-free bovine serum albumin, the negative control, ~66.5 kDa) were examined using a Biacore X100 (BR110073) equipped with research-grade streptavidin (SA)-coated sensor chips (Cityva, England) at 25 °C.

Following the manufacturer's recommendations, the SA-coated sensor chips were preconditioned with 1 M NaCl in 50 mM NaOH and then washed with 50% dimethyl carbinol, 1 M NaCl in 50 mM NaOH to ensure a clean surface.

The biotinylated NsrP promoter DNA was immobilized at a flow rate of 30 $\mu\text{L}/\text{min}$ using 100 $\mu\text{g}/\text{mL}$ DNA oligonucleotides diluted in 1 \times HBS-EP+ running buffer, generating low-density surfaces with approximately 1000 response units (RU). Lrp or BSA at concentrations ranging from 20 nM to 1.25 μM was injected over the active surface containing NsrP promoter DNA using the Kinetics/Affinity mode at a flow rate of 30 $\mu\text{L}/\text{min}$. The association phase lasted for 180 s, followed by a 300-s dissociation phase.

Between sample injections, surfaces were regenerated at a flow rate of 30 $\mu\text{L}/\text{min}$ using two 30 s pulses of 0.5% [vol/vol] SDS solution, followed by Extra-clean and Rinse procedures as specified by the instrument protocol. The Biacore X100 evaluation software was used to fit the affinity curves using a steady-state affinity model. The equilibrium dissociation constant (KD) was calculated.

Bacterial growth curve assays

Overnight cultures were used to seed in M9 minimal medium with or without 40 mM IMP at an optical density at 600 nm (OD_{600}) of 0.1 as previously described²². A 200 μL aliquot was added to a 96-well microplate and incubated at 37 °C with shaking at 180 rpm for 24 h. The OD_{600} was recorded every 20 min. Experiments were independently performed three times.

Lux-based light production measurements

The DNA fragment containing *purDH* promoter and full length of *purDH* or *purD^{mutH}* were amplified, purified, and digested with BamHI/HindIII. The products were ligated to pMS402 plasmid, respectively, to construct *lux* fusion plasmids. The DNA fragments of NsrP and NsrP^{mut} (AAUUACU to UUAAGA) were amplified, purified, digested with MscI/EcoRI and ligated to pNM12 plasmid, respectively, to construct sRNA overexpression plasmids. The empty pNM12 vector was labeled as control. The plasmids and insertions were verified by colony PCR and Sanger sequencing. Single colonies of ΔNsrP strains harboring *lux* fusions and sRNA overexpression plasmids were grown to logarithmic phase in LB medium at 37 °C, and then incubated with 0.1% of arabinose for 30 min to induce the expression of NsrP or NsrP^{mut}. The luminescence was measured using the Spark multimode microplate reader (Tecan).

Northern blotting

Northern blotting was performed using the DIG Northern Starter kit (Roche). About 15 μg total RNA were electrophoresed in a 1.2% agarose gel containing 37% formaldehyde. RNA was transferred to nitrocellulose membranes and immobilized at 120 °C for 30 min. Prehybridization was performed in digoxigenin (DIG) Easy Hyb buffer for 30 min. The DIG-labeled RNA probe was added and incubated overnight. The membrane was washed twice in 2 \times SSC/0.1% SDS for 5 min at room temperature and followed by 1 \times SSC/0.1% SDS buffers for 15 min at 68 °C. Signals were visualized using an Amersham Imager 680, 5S rRNA being used as an internal control.

Western blotting

LB-cultured NMEC, ΔNsrP , and cNsrP strains grown to the logarithmic phase were pelleted and lysed to obtain total protein. The proteins (100 μg) were separated by 10% SDS-PAGE and transferred to polyvinylidene difluoride membranes. The membranes were blocked with Tris-buffered saline with 0.1% (w/v) Tween 20 (TBST) containing 5% skim milk for 1 h at room temperature. The membranes were then incubated with the primary antibody anti-FLAG (1:1000 dilution, Sigma, F1804) and DnaK (1:1000 dilution, Abcam, ab69617) overnight at 4 °C followed by the secondary antibody Goat Anti-Mouse IgG H&L-

HRP (1:5000 dilution, Abcam, ab6789) for 1 h at room temperature. Samples were visualized with chemiluminescence and the protein levels were analyzed using ImageJ which normalized to DnaK from three independent experiments.

ChIP and ChIP-qPCR

The pTRC99A-Lrp-3 \times FLAG recombinant plasmid was electroporated into Δlrp . The LB-cultured Δlrp containing pTRC99A-Lrp-3 \times FLAG grown up to late-logarithmic phase was treated with 1% formaldehyde for 25 min at room temperature. The reaction was quenched by the addition of 0.5 M glycine and sonicated to generate DNA fragments of 200–500 bp. The sample was pelleted, and the supernatant was used for immunoprecipitation with an anti-3 \times FLAG antibody (Sigma, F1804) and protein A magnetic beads (Invitrogen, 10002D) according to the manufacturer's instructions. An aliquot without antibody served as negative control (Mock). The sample then was incubated with RNaseA for 2 h at 37 °C, and proteinase K for 2 h at 55 °C. DNA fragments were purified using a PCR purification kit (Roche, 11732668001). The relative enrichment of the promoter of NsrP and *rpoS* (the negative control) was examined with qRT-PCR as mentioned above and *rpoA* gene was used as reference control.

Animal experiments

Two- to 5-day-old Sprague-Dawley in both sexes and 18-day-old BALB/c male mice were purchased from Beijing Vital River Laboratory Animal Technology Co., Ltd. (licensed by Charles River), and housed in a temperature-controlled room in a specific pathogen-free facility with a 12 h light/12 h dark cycle. 18-day-old BALB/c mice were used for the experimental hematogenous meningitis model, in which animals develop a high level of bacteremia followed by bacterial traversal of the BBB mimicking the pathogenesis of human *E. coli* meningitis¹⁸. Two- to 5-day-old Sprague-Dawley rats were used for intestine colonization assays and mouse survival assays as previously described^{27,28}. For the experimental hematogenous meningitis model, each mouse received 1×10^6 CFU of NMEC WT or mutant strains in the logarithmic phase of growth via the tail vein. Four hours later, blood and CSF specimens were collected for bacterial cultures (CFU). For the leucine administration assay, L-leucine (10 mg/mL) or PBS was administered via the tail vein injection at a dose of 1 mg/30 g body weight at 0.5 h post-infection of NMEC⁶⁸. For intestine colonization assays, 2- to 5-day-old Sprague-Dawley rats were orally infected by pipette feeding of 20 μL PBS containing 2×10^6 CFU of NMEC WT or mutant strains in the logarithmic phase of growth. Small intestine specimens were collected following the contents were removed after 24 h infection, then weighed, washed with PBS, and homogenized for bacterial cultures. The in vivo colonization efficiency was determined by counting the number of CFU per g of tissues²⁸. For mouse survival assays, 2- to 5-day-old Sprague-Dawley rats were subcutaneously injected with 1×10^5 CFU of NMEC WT or mutant strains in the logarithmic phase of growth²⁷. The number of animals alive was recorded every 8 h.

E. coli invasion assay in HBMEC

Immortalized cell line HBMEC were a generous gift from Dr. K.S. Kim (Johns Hopkins University, Baltimore, MD). The immortalized HBMECs have been verified for their function and morphological structure, which are similar to primary cells⁶⁹. *E. coli* invasion into HBMECs were assessed as described^{17,70}. HBMECs were cultured in Dulbecco's Modified Eagle Medium (DMEM, Gibco) supplemented with 10% fetal bovine serum and 10% Nu-Serum (BD Biosciences) at 37 °C in 5% CO_2 . The NMEC WT or mutant strains in the logarithmic phase of growth were collected and resuspended in an experimental medium (M199-HamF12 [1:1], containing 5% heat-inactivated fetal bovine serum, 2 mM

glutamine, and 1 mM pyruvate). HBMEC grown in collagen-coated 24-well plates were infected with the suspension in a multiplicity of infection of 100:1 and incubated at 37 °C in 5% CO₂ for 90 min. HBMEC were washed with PBS three times and reincubated with an experimental medium containing gentamicin (100 mg/ml) for 1 h at 37 °C in 5% CO₂ to kill extracellular bacteria before the cells were lysed. The lysates were plated on LB agar plates and cultured overnight to count the bacterial CFU for quantifications³. The results were expressed as percent relative invasion compared to the percent invasion of NMEC WT.

Analysis of the distribution of NsrP in *E. coli*

930 *E. coli* complete genomes containing 46 NMEC strains, 77 Uropathogenic *E. coli* (UPEC) strains, 85 Enteropathogenic *E. coli* (EPEC) strains, 366 EHEC strains, and 356 nonpathogenic *E. coli* strains were downloaded from the GenBank database at the National Center for Biotechnology Information (NCBI) (<https://www.ncbi.nlm.nih.gov/genbank/>). NsrP was identified using blastn (minimum sequence coverage/identify 80/85%).

Quantification and statistical analysis

Data are shown as bar graphs or dot plots (means ± SDs) of three independent experiments. Statistical significance was analyzed with GraphPad Prism 9.5.0 software (GraphPad Inc) using the two-tailed unpaired Student's *t*-test, one-way ANOVA, two-way ANOVA, log-rank (Mantel-Cox) test, or Mann-Whitney *U*-test according to the test requirements, as stated in the figure legends.

Reporting summary

Further information on research design is available in the Nature Portfolio Reporting Summary linked to this article.

Data availability

All study data were available in the main text and/or Supplementary information. Source data are provided with this paper.

References

- van de Beek, D., Brouwer, M. C., Koedel, U. & Wall, E. C. Community-acquired bacterial meningitis. *Lancet* **398**, 1171–1183 (2021).
- van de Beek, D., de Gans, J., Tunkel, A. R. & Wijdicks, E. F. Community-acquired bacterial meningitis in adults. *N. Engl. J. Med.* **354**, 44–53 (2006).
- Zhao, W. D. et al. Caspr1 is a host receptor for meningitis-causing *Escherichia coli*. *Nat. Commun.* **9**, 2296 (2018).
- Kim, K. S. Human meningitis-associated *Escherichia coli*. *EcoSal Plus* **7**, ESP-0015-2015 (2016).
- Kim, K. S. Acute bacterial meningitis in infants and children. *Lancet Infect. Dis.* **10**, 32–42 (2010).
- Kim, K. S. Pathogenesis of bacterial meningitis: from bacteraemia to neuronal injury. *Nat. Rev. Neurosci.* **4**, 376–385 (2003).
- Croxen, M. A. & Finlay, B. B. Molecular mechanisms of *Escherichia coli* pathogenicity. *Nat. Rev. Microbiol.* **8**, 26–38 (2010).
- Doran, K. S. et al. Host-pathogen interactions in bacterial meningitis. *Acta Neuropathol* **131**, 185–209 (2016).
- Xie, Y., Kim, K. J. & Kim, K. S. Current concepts on *Escherichia coli* K1 translocation of the blood-brain barrier. *FEMS Immunol. Med. Microbiol.* **42**, 271–279 (2004).
- Rossi, E. & La Rosa, R. *Pseudomonas aeruginosa* adaptation and evolution in patients with cystic fibrosis. *Nat. Rev. Microbiol.* **19**, 331–342 (2021).
- Storz, G., Vogel, J. & Wassarman, K. M. Regulation by small RNAs in bacteria: expanding frontiers. *Mol. Cell* **43**, 880–891 (2011).
- Sauder, A. B. & Kendall, M. M. After the fact(or): posttranscriptional gene regulation in enterohemorrhagic *Escherichia coli* O157:H7. *J. Bacteriol.* **200**, e00228–18 (2018).
- Melson, E. M. & Kendall, M. M. The sRNA DicF integrates oxygen sensing to enhance enterohemorrhagic *Escherichia coli* virulence via distinctive RNA control mechanisms. *Proc. Natl Acad. Sci. USA* **116**, 14210–14215 (2019).
- Jia, T. et al. A novel small RNA promotes motility and virulence of enterohemorrhagic *Escherichia coli* O157:H7 in response to ammonium. *mBio* **12**, e03605–e03620 (2021).
- Jia, T. & Wu, P. The phosphate-induced small RNA EsrL promotes *E. coli* virulence, biofilm formation, and intestinal colonization. *Sci. Signal.* **16**, eabm0488 (2023).
- Sauder, A. B. & Kendall, M. M. A pathogen-specific sRNA influences enterohemorrhagic *Escherichia coli* fitness and virulence in part by direct interaction with the transcript encoding the ethanolamine utilization regulatory factor EutR. *Nucleic Acids Res.* **49**, 10988–11004 (2021).
- Sun, H. et al. An ArcA-modulated small RNA in pathogenic *Escherichia coli* K1. *Front. Microbiol.* **11**, 574833 (2020).
- Sun, H. et al. Bacteria reduce flagellin synthesis to evade microglia-astrocyte-driven immunity in the brain. *Cell Rep.* **40**, 111033 (2022).
- Xie, Y. et al. Identification and characterization of *Escherichia coli* RS218-derived islands in the pathogenesis of *E. coli* meningitis. *J. Infect. Dis.* **194**, 358–364 (2006).
- Goncheva, M. I., Chin, D. & Heinrichs, D. E. Nucleotide biosynthesis: the base of bacterial pathogenesis. *Trends Microbiol.* **30**, 793–804 (2022).
- Kim, G. L. et al. Growth and stress tolerance comprise independent metabolic strategies critical for *Staphylococcus aureus* infection. *mBio* **12**, e0081421 (2021).
- Shaffer, C. L. et al. Purine biosynthesis metabolically constrains intracellular survival of uropathogenic *Escherichia coli*. *Infect. Immun.* **85**, e00471–16 (2017).
- Connolly, J. et al. Identification of *Staphylococcus aureus* factors required for pathogenicity and growth in human blood. *Infect. Immun.* **85**, e00337–17 (2017).
- Samant, S. et al. Nucleotide biosynthesis is critical for growth of bacteria in human blood. *PLoS Pathog.* **4**, e37 (2008).
- Zhang, Y., Morar, M. & Ealick, S. E. Structural biology of the purine biosynthetic pathway. *Cell. Mol. Life Sci.* **65**, 3699–3724 (2008).
- Teng, C. H. et al. Nlpl contributes to *Escherichia coli* K1 strain RS218 interaction with human brain microvascular endothelial cells. *Infect. Immun.* **78**, 3090–3096 (2010).
- Zhang, X. W. et al. Lpp of *Escherichia coli* K1 inhibits host ROS production to counteract neutrophil-mediated elimination. *Redox Biol.* **59**, 102588 (2023).
- McCarthy, A. J. & Stabler, R. A. Genome-wide identification by transposon insertion sequencing of *Escherichia coli* K1 genes essential for in vitro growth, gastrointestinal colonizing capacity, and survival in serum. *J. Bacteriol.* **200**, e00698–17 (2018).
- Mei, J. M., Nourbakhsh, F., Ford, C. W. & Holden, D. W. Identification of *Staphylococcus aureus* virulence genes in a murine model of bacteraemia using signature-tagged mutagenesis. *Mol. Microbiol.* **26**, 399–407 (1997).
- Aiba, A. & Mizobuchi, K. Nucleotide sequence analysis of genes *purH* and *purD* involved in the de novo purine nucleotide biosynthesis of *Escherichia coli*. *J. Biol. Chem.* **264**, 21239–21246 (1989).
- Hart, B. R. & Blumenthal, R. M. Unexpected coregulator range for the global regulator Lrp of *Escherichia coli* and *Proteus mirabilis*. *J. Bacteriol.* **193**, 1054–1064 (2011).
- Yokoyama, K. et al. Feast/famine regulation by transcription factor FL11 for the survival of the hyperthermophilic archaeon *Pyrococcus OT3*. *Structure* **15**, 1542–1554 (2007).
- Nhu, N. T. K. & Phan, M. D. High-risk *Escherichia coli* clones that cause neonatal meningitis and association with recrudescence infection. *eLife* **12**, RP91853 (2024).

34. Dallas, D. C. et al. Personalizing protein nourishment. *Crit. Rev. Food Sci. Nutr.* **57**, 3313–3331 (2017).
35. Solmonson, A. & Faubert, B. Compartmentalized metabolism supports midgestation mammalian development. *Nature* **604**, 349–353 (2022).
36. Thorell, L., Sjöberg, L. B. & Hernell, O. Nucleotides in human milk: sources and metabolism by the newborn infant. *Pediatr. Res.* **40**, 845–852 (1996).
37. Malo, C. Free amino acid levels in serum and small intestine during the post-natal development of normal and sparse-fur mutant mice. *Comp. Biochem. Physiol. A Physiol.* **109**, 1049–1057 (1994).
38. Gripenland, J. et al. RNAs: regulators of bacterial virulence. *Nat. Rev. Microbiol.* **8**, 857–866 (2010).
39. Gruber, C. C. & Sperandio, V. Global analysis of posttranscriptional regulation by GlmY and GlmZ in enterohemorrhagic *Escherichia coli* O157:H7. *Infect. Immun.* **83**, 1286–1295 (2015).
40. Wu, K. et al. RNA interactome of hypervirulent *Klebsiella pneumoniae* reveals a small RNA inhibitor of capsular mucoviscosity and virulence. *Nat. Commun.* **15**, 6946 (2024).
41. Hoang, T. M., Huang, W., Gans, J. & Weiner, J. The heme-responsive PrrH sRNA regulates *Pseudomonas aeruginosa* pyochelin gene expression. *mSphere* **8**, e0039223 (2023).
42. Briones, A. C. et al. Genetic regulation of the *ompX* porin of *Salmonella Typhimurium* in response to hydrogen peroxide stress. *Biol. Res.* **55**, 8 (2022).
43. Cao, P., Fleming, D. & Moustafa, D. A. A *Pseudomonas aeruginosa* small RNA regulates chronic and acute infection. *Nature* **618**, 358–364 (2023).
44. Juhas, M. Horizontal gene transfer in human pathogens. *Crit. Rev. Microbiol.* **41**, 101–108 (2015).
45. Frost, L. S., Lepaie, R., Summers, A. O. & Toussaint, A. Mobile genetic elements: the agents of open source evolution. *Nat. Rev. Microbiol.* **3**, 722–732 (2005).
46. Koonin, E. V. & Wolf, Y. I. Genomics of bacteria and archaea: the emerging dynamic view of the prokaryotic world. *Nucleic Acids Res.* **36**, 6688–6719 (2008).
47. Konczyk, P. et al. Genomic O island 122, locus for enterocyte effacement, and the evolution of virulent verocytotoxin-producing *Escherichia coli*. *J. Bacteriol.* **190**, 5832–5840 (2008).
48. Ziegler, C. A. & Freddolino, P. L. The leucine-responsive regulatory proteins/feast-famine regulatory proteins: an ancient and complex class of transcriptional regulators in bacteria and archaea. *Crit. Rev. Biochem. Mol. Biol.* **56**, 373–400 (2021).
49. Ihara, K. et al. Expression of the *alaE* gene is positively regulated by the global regulator Lrp in response to intracellular accumulation of L-alanine in *Escherichia coli*. *J. Biosci. Bioeng.* **123**, 444–450 (2017).
50. Trouillon, J., Doubleday, P. F. & Sauer, U. Genomic footprinting uncovers global transcription factor responses to amino acids in *Escherichia coli*. *Cell Syst* **14**, 860–871 (2023).
51. Chen, S., Iannolo, M. & Calvo, J. M. Cooperative binding of the leucine-responsive regulatory protein (Lrp) to DNA. *J. Mol. Biol.* **345**, 251–264 (2005).
52. Geslain, G. et al. Genome sequencing of strains of the most prevalent clonal group of O1:K1:H7 *Escherichia coli* that causes neonatal meningitis in France. *BMC Microbiol.* **19**, 17 (2019).
53. Sáez-López, E. et al. Outbreak caused by *Escherichia coli* O18: K1: H7 sequence type 95 in a neonatal intensive care unit in Barcelona, Spain. *Pediatr. Infect. Dis. J.* **36**, 1079–1086 (2017).
54. Barichello, T. et al. Bacterial meningitis in Africa. *Front. Neurol.* **14**, 822575 (2023).
55. Zhang, Q., Cheng, L., Wang, J., Hao, M. & Che, H. Antibiotic-induced gut microbiota dysbiosis damages the intestinal barrier, increasing food allergy in adult mice. *Nutrients* **13**, 3315 (2021).
56. Duan, Y. et al. Antibiotic resistance and virulence of extraintestinal pathogenic *Escherichia coli* (ExPEC) vary according to molecular types. *Front. Microbiol.* **11**, 598305 (2020).
57. Leenders, M. & van Loon, L. J. Leucine as a pharmaconutrient to prevent and treat sarcopenia and type 2 diabetes. *Nutr. Rev.* **69**, 675–689 (2011).
58. De Bandt, J. P. & Cynober, L. Therapeutic use of branched-chain amino acids in burn, trauma, and sepsis. *J. Nutr.* **136**, 308s–313s (2006).
59. Holecek, M. Branched-chain amino acids and ammonia metabolism in liver disease: therapeutic implications. *Nutrition* **29**, 1186–1191 (2013).
60. Borack, M. S. & Volpi, E. Efficacy and safety of leucine supplementation in the elderly. *J. Nutr.* **146**, 2625s–2629s (2016).
61. Bauer, J. M. et al. Effects of a vitamin D and leucine-enriched whey protein nutritional supplement on measures of sarcopenia in older adults, the PROVIDE study: a randomized, double-blind, placebo-controlled trial. *J. Am. Med. Dir. Assoc.* **16**, 740–747 (2015).
62. Lo, J. H., U, K. P., Yiu, T., Ong, M. T. & Lee, W. Y. Sarcopenia: current treatments and new regenerative therapeutic approaches. *J. Orthop. Translat.* **23**, 38–52 (2020).
63. Huang, S. H. et al. Identification and characterization of an *Escherichia coli* invasion gene locus, *ibeB*, required for penetration of brain microvascular endothelial cells. *Infect. Immun.* **67**, 2103–2109 (1999).
64. Datsenko, K. A. & Wanner, B. L. One-step inactivation of chromosomal genes in *Escherichia coli* K-12 using PCR products. *Proc. Natl Acad. Sci. USA* **97**, 6640–6645 (2000).
65. McClure, R. et al. Computational analysis of bacterial RNA-Seq data. *Nucleic Acids Res.* **41**, e140 (2013).
66. Mann, B. et al. Control of virulence by small RNAs in *Streptococcus pneumoniae*. *PLoS Pathog.* **8**, e1002788 (2012).
67. Bradford, M. M. A rapid and sensitive method for the quantitation of microgram quantities of protein utilizing the principle of protein-dye binding. *Anal. Biochem.* **72**, 248–254 (1976).
68. Ma, C. et al. L-leucine promotes axonal outgrowth and regeneration via mTOR activation. *FASEB J.* **35**, e21526 (2021).
69. Stins, M. F., Badger, J. & Sik Kim, K. Bacterial invasion and transcytosis in transfected human brain microvascular endothelial cells. *Microb. Pathog.* **30**, 19–28 (2001).
70. Zhu, L. et al. Arachidonic acid metabolism regulates *Escherichia coli* penetration of the blood-brain barrier. *Infect. Immun.* **78**, 4302–4310 (2010).

Acknowledgements

This work was supported by the National Natural Science Foundation of China Program under Grant No. 82402643 (to H.S.), 32070130 (to B.L.), 82372267 (to B.L.), 32070133 (to L.F.), 32470111 (to L.F.), 32130003 (to L.W.), 32370194 (to L.W.); the Natural Science Foundation of Shenzhen under Grant No. JCYJ20220530164604010 (to B.L.), JCYJ20230807151559009 (to B.L.); Guangdong Basic and Applied Basic Research Foundation Grant 2024A151010588 (to B.L.); Shenzhen Science and Technology Program Grant JCYJ20210324135007019 (to L.F.); Key Laboratory Major Project of 2024 (Tianjin) Grant 24ZXZSSS00140 (to B.L.), and Fundamental Research Funds for Central Universities under Grant No. 63233172 (to B.L.).

Author contributions

Conceptualization, B.L., H.S., and X.L.; methodology, H.S., X.L., X.Y., J.Q., Y.L., Y.Z., H.S., Q.W., R.L., X.C., Q.Z., T.J., and X.W.; visualization, H.S., X.L., and X.Y.; supervision, B.L.; writing—original draft, B.L., H.S., and X.L.; writing—review and editing, B.L., H.S., X.L., L.F., and L.W.

Competing interests

The authors declare no competing interests.

Additional information

Supplementary information The online version contains supplementary material available at <https://doi.org/10.1038/s41467-025-57850-2>.

Correspondence and requests for materials should be addressed to Lei Wang or Bin Liu.

Peer review information *Nature Communications* thanks Sahar Melamed, Andrew Roe and the other, anonymous, reviewer(s) for their contribution to the peer review of this work. A peer review file is available.

Reprints and permissions information is available at <http://www.nature.com/reprints>

Publisher's note Springer Nature remains neutral with regard to jurisdictional claims in published maps and institutional affiliations.

Open Access This article is licensed under a Creative Commons Attribution-NonCommercial-NoDerivatives 4.0 International License, which permits any non-commercial use, sharing, distribution and reproduction in any medium or format, as long as you give appropriate credit to the original author(s) and the source, provide a link to the Creative Commons licence, and indicate if you modified the licensed material. You do not have permission under this licence to share adapted material derived from this article or parts of it. The images or other third party material in this article are included in the article's Creative Commons licence, unless indicated otherwise in a credit line to the material. If material is not included in the article's Creative Commons licence and your intended use is not permitted by statutory regulation or exceeds the permitted use, you will need to obtain permission directly from the copyright holder. To view a copy of this licence, visit <http://creativecommons.org/licenses/by-nc-nd/4.0/>.

© The Author(s) 2025